International Journal of
Molecular Sciences

MDPI

Article

Scandium Ion-Promoted Electron-Transfer Disproportionation of 2-Phenyl-4,4,5,5-tetramethylimidazoline-1-oxyl 3-Oxide (PTIO•) in Acetonitrile and Its Regeneration Induced by Water

Yoshimi Shoji [1], Yuri Terashima [2], Kei Ohkubo [3,†], Hiromu Ito [1], Kouichi Maruyama [2], Shunichi Fukuzumi [4,5,†] and Ikuo Nakanishi [1,*]

[1] Quantum RedOx Chemistry Team, Institute for Quantum Life Science (iQLS), Quantum Life and Medical Science Directorate (QLMS), National Institutes for Quantum Science and Technology (QST), Chiba-shi 263-8555, Chiba, Japan; shoji.yoshimi@qst.go.jp (Y.S.); ito.hiromu@qst.go.jp (H.I.)
[2] Environmental Radiation Effects Research Group, Department of Radiation Measurement and Dose Assessment, Institute for Radiological Science (NIRS), Quantum Life and Medical Science Directorate (QLMS), National Institutes for Quantum Science and Technology (QST), Chiba-shi 263-8555, Chiba, Japan; terashima.yuri@qst.go.jp (Y.T.); maruyama.kouichi@qst.go.jp (K.M.)
[3] Institute for Advanced Co-Creation Studies, Open and Transdisciplinary Research Initiatives, Osaka University, Suita 565-0871, Osaka, Japan; ohkubo@irdd.osaka-u.ac.jp
[4] Department of Chemistry and Nano Science, Ewha Womans University, Seoul 03760, Republic of Korea; fukuzumi@chem.eng.osaka-u.ac.jp
[5] Department of Chemistry, Faculty of Pure and Applied Sciences, University of Tsukuba, Tsukuba 305-8571, Ibaraki, Japan
* Correspondence: nakanishi.ikuo@qst.go.jp; Tel.: +81-43-206-3131
† These authors contributed equally to this work.

Abstract: 2-Phenyl-4,4,5,5-tetramethylimidazoline-1-oxyl 3-oxide (PTIO•), a persistent nitronyl nitroxide radical, has been used for the detection and trapping of nitric oxide, as a redox mediator for batteries, for the activity estimation of antioxidants, and so on. However, there is no report on the reactivity of PTIO• in the presence of redox-inactive metal ions. In this study, it is demonstrated that the addition of scandium triflate, $Sc(OTf)_3$ (OTf = OSO_2CF_3), to an acetonitrile (MeCN) solution of PTIO• resulted in an electron-transfer disproportionation to generate the corresponding cation ($PTIO^+$) and anion ($PTIO^-$), the latter of which is suggested to be stabilized by Sc^{3+} to form $[(PTIO)Sc]^{2+}$. The decay of the absorption band at 361 nm due to PTIO•, monitored using a stopped-flow technique, obeyed second-order kinetics. The second-order rate constant for the disproportionation, thus determined, increased with increasing the $Sc(OTf)_3$ concentration to reach a constant value. A drastic change in the cyclic voltammogram recorded for PTIO• in deaerated MeCN containing 0.10 M Bu_4NClO_4 was also observed upon addition of $Sc(OTf)_3$, suggesting that the large positive shift of the one-electron reduction potential of PTIO• (equivalent to the one-electron oxidation potential of $PTIO^-$) in the presence of $Sc(OTf)_3$ may result in the disproportionation. When H_2O was added to the PTIO•–$Sc(OTf)_3$ system in deaerated MeCN, PTIO• was completely regenerated. It is suggested that the complex formation of Sc^{3+} with H_2O may weaken the interaction between $PTIO^-$ and Sc^{3+}, leading to electron-transfer comproportionation to regenerate PTIO•. The reversible disproportionation of PTIO• was also confirmed by electron paramagnetic resonance (EPR) spectroscopy.

Keywords: radical; electron transfer; disproportionation; scandium ion; Lewis acid; comproportionation; kinetics; reaction mechanism; cyclic voltammetry; electron paramagnetic resonance

check for updates

Citation: Shoji, Y.; Terashima, Y.; Ohkubo, K.; Ito, H.; Maruyama, K.; Fukuzumi, S.; Nakanishi, I. Scandium Ion-Promoted Electron-Transfer Disproportionation of 2-Phenyl-4,4,5,5-tetramethylimidazoline-1-oxyl 3-Oxide (PTIO•) in Acetonitrile and Its Regeneration Induced by Water. *Int. J. Mol. Sci.* **2024**, *25*, 4417. https://doi.org/10.3390/ijms25084417

Academic Editor: Wolfgang Linert

Received: 20 March 2024
Revised: 9 April 2024
Accepted: 16 April 2024
Published: 17 April 2024

Copyright: © 2024 by the authors. Licensee MDPI, Basel, Switzerland. This article is an open access article distributed under the terms and conditions of the Creative Commons Attribution (CC BY) license (https://creativecommons.org/licenses/by/4.0/).

1. Introduction

Redox-inactive metal ions have attracted much attention because they are known to affect the redox behavior of redox active compounds acting as a Lewis acid [1–9]. Among such metal ions, scandium ion (Sc^{3+}) shows the strongest Lewis acidity because of the

small ionic radius with trivalent positive charge, leading to a significant positive shift of the reduction potentials of compounds [10–23], including metal–oxygen complexes [19–21] and radical species [22,23]. Of special interest is the fact that Sc^{3+} enables the electron-transfer reactions, which would otherwise never take place in the absence of Sc^{3+}, to occur thermodynamically as well as kinetically [10–15,20,21]. We have reported that an electron-transfer disproportionation of 2,2-diphenyl-1-picrylhydrazyl radical ($DPPH^{\bullet}$) occurs upon the addition of scandium triflate, $Sc(OTf)_3$ (OTf = OSO_2CF_3), to an acetonitrile (MeCN) solution of $DPPH^{\bullet}$ to produce one-electron-oxidized and -reduced species of $DPPH^{\bullet}$, $DPPH^{+}$, and $DPPH^{-}$, respectively [23]. The spectral titration showed that four molecules of $DPPH^{\bullet}$ react with Sc^{3+} to produce two molecules of $DPPH^{+}$ and a complex between two molecules of $DPPH^{-}$ and Sc^{3+}, $[(DPPH)_2Sc]^{+}$ [24]. Further, it is also reported that the addition of H_2O to the $DPPH^{\bullet}$–$Sc(OTf)_3$ system in MeCN resulted in the regeneration of $DPPH^{\bullet}$ [24]. Very recently, a similar reversible disproportionation reaction has been reported for 2,2,6,6-tetramethylpiperidyl-1-oxyl (TEMPO) in the presence of $Al(OTf)_3$ to develop an aqueous aluminum radical batteries [25]. Dedzo et al. have also reported drastic changes in the redox reactivity of $DPPH^{\bullet}$ in the presence of metal cations, such as Cu^{2+} and Zn^{2+}, as well as Brønsted acid, such as $HClO_4$ and HNO_3 [8].

On the other hand, 2-phenyl-4,4,5,5-tetramethylimidazoline-1-oxyl 3-oxide ($PTIO^{\bullet}$) (Scheme 1), a persistent nitronyl nitroxide radical, has been used for the detection and trapping of nitric oxide ($^{\bullet}NO$) for about 30 years [26–34]. Furthermore, $PTIO^{\bullet}$ has also attracted much attention as a redox mediator for batteries [35–37]. Recently, it has been reported that $PTIO^{\bullet}$ can be used to estimate the activity of antioxidants as a reactivity model of reactive oxygen species [38–57]. However, there is no report on the reactivity of $PTIO^{\bullet}$ in the presence of redox-inactive metal ions. $PTIO^{\bullet}$ shows a similar reversible one-electron redox behavior (Scheme 1) to $DPPH^{\bullet}$, although the separation between the one-electron oxidation and reduction potentials of $PTIO^{\bullet}$ (1.73 V) [35] is much larger than that of $DPPH^{\bullet}$ (0.52 V) [23]. We report herein that an electron-transfer disproportionation of $PTIO^{\bullet}$ also occurs upon the addition of $Sc(OTf)_3$ to a deaerated MeCN solution of $PTIO^{\bullet}$. Also studied was the regeneration of $PTIO^{\bullet}$ upon the addition of H_2O to the $PTIO^{\bullet}$–$Sc(OTf)_3$ system in deaerated MeCN. The drastic change in the redox behavior of compounds due to the strong Lewis acidity of Sc^{3+} observed in this study provides valuable and fundamental information about the fine tuning of the redox reactions by the redox-inactive metal ions.

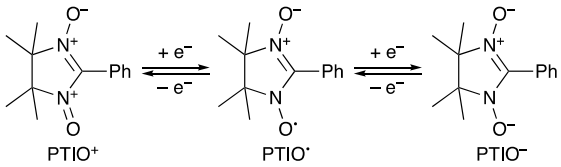

Scheme 1. Redox behavior of $PTIO^{\bullet}$.

2. Results and Discussion

When $Sc(OTf)_3$ was added to a deaerated MeCN solution of $PTIO^{\bullet}$, the absorption bands at 238, 264, and 361 nm and a broad band at around 600 nm due to $PTIO^{\bullet}$ decreased immediately with clear isosbestic points at 277, 334, 381, and 525 nm, as shown in Figure 1 (Video S1 of the Supplementary Materials). The broad absorption band at 450 nm is diagnostic of the one-electron-oxidized $PTIO^{\bullet}$ ($PTIO^{+}$) [33]. Thus, an electron-transfer disproportionation of $PTIO^{\bullet}$ is suggested to take place upon addition of $Sc(OTf)_3$ to produce $PTIO^{+}$ and the one-electron-reduced $PTIO^{\bullet}$ ($PTIO^{-}$), as in the case of $DPPH^{\bullet}$ [23]. The spectral titration (inset of Figure 1) shows the $Sc(OTf)_3$/$PTIO^{\bullet}$ molar ratio being 1:2. This suggests that one molecule of $PTIO^{-}$ may be stabilized by one Sc^{3+} (Scheme 2). When MeCN was replaced by methanol (MeOH) or ethanol (EtOH) as the solvent, such a spectral change was not observed. This suggests that the stronger solvation of Sc^{3+} in MeOH or EtOH compared to that in MeCN may preclude the disproportionation from occurring.

$$2PTIO^{\bullet} + Sc^{3+} \longrightarrow PTIO^{+} + [(PTIO)Sc]^{2+}$$

Scheme 2. Sc^{3+}-promoted electron-transfer disproportionation of $PTIO^{\bullet}$.

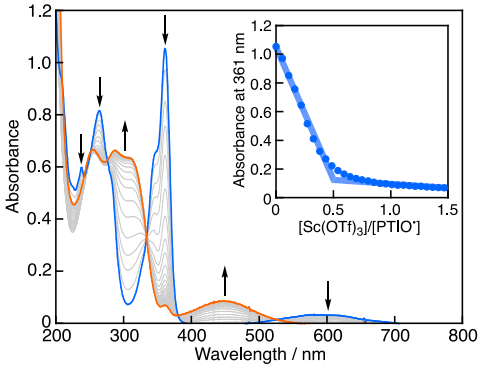

Figure 1. Spectral change observed upon addition of $Sc(OTf)_3$ (4.4×10^{-6} M each) to $PTIO^{\bullet}$ (7.2×10^{-5} M) in deaerated MeCN. Blue and orange lines are the initial and final spectra, respectively. Arrows denote the direction of absorption changes. Inset: plot of the absorbance at 361 nm vs. $[Sc(OTf)_3]/[PTIO^{\bullet}]$.

The spectral change after the addition of $Sc(OTf)_3$ (7.9×10^{-3} M) to a deaerated MeCN solution of $PTIO^{\bullet}$ (5.5×10^{-5} M) monitored by a stopped-flow technique is shown in Figure 2a. The time course change in the absorbance at 361 nm obeyed second-order kinetics (inset of Figure 2a). The observed second-order rate constant (k_{disp}, disp: disproportionation) was determined by a decrease in absorbance at 361 nm due to $PTIO^{\bullet}$. The k_{disp} value increases with increasing concentration of $Sc(OTf)_3$ ($[Sc(OTf)_3]$) to reach a constant value (Figure 2b). The limiting k_{disp} value (k_{∞}) and the binding constant (K) between $PTIO^{\bullet}$ and Sc^{3+} were determined from curve fitting based on Scheme 3 and Equation (1) to be 9.3×10^4 M^{-1} s^{-1} and 1.0×10^3 M^{-1}, respectively.

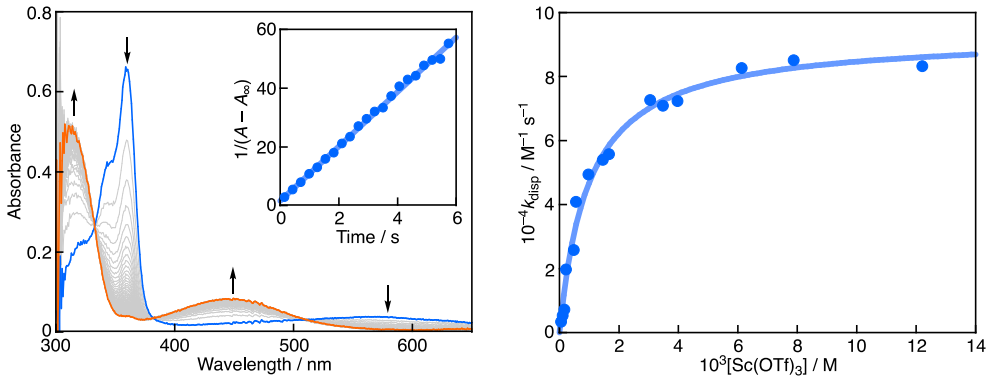

(**a**) (**b**)

Figure 2. (**a**) Spectral change (interval: 70 ms) observed during the reaction of $PTIO^{\bullet}$ (5.5×10^{-5} M) with $Sc(OTf)_3$ (7.9×10^{-3} M) in deaerated MeCN at 298 K. Blue and orange lines are the initial and final spectra, respectively. Arrows denote the direction of absorption changes. Inset: the second-order plot of the absorbance at 361 nm. (**b**) Plot of k_{disp} vs. $[Sc(OTf)_3]$ for the disproportionation of $PTIO^{\bullet}$ (5.5×10^{-5} M) in the presence of $Sc(OTf)_3$ in deaerated MeCN at 298 K.

$$PTIO^{\bullet} + Sc^{3+} \underset{}{\overset{K}{\rightleftharpoons}} [(PTIO^{\bullet})Sc]^{3+} \xrightarrow[k_{\infty}]{PTIO^{\bullet}} PTIO^{+} + [(PTIO)Sc]^{2+}$$

Scheme 3. Proposed mechanism of the Sc^{3+}-promoted electron-transfer disproportionation of $PTIO^{\bullet}$.

According to Equation (1), when [$Sc(OTf)_3$] is low (1 >> K[$Sc(OTf)_3$]), the k_{disp} value increases with increasing [$Sc(OTf)_3$]. On the other hand, when [$Sc(OTf)_3$] is high enough to produce [(PTIO$^{\bullet}$)Sc]$^{3+}$, the reaction between PTIO$^{\bullet}$ and [(PTIO$^{\bullet}$)Sc]$^{3+}$ becomes the rate-determining step and the k_{disp} value reaches k_{∞}.

$$k_{disp} = k_{\infty}K[Sc(OTf)_3]/(1 + K[Sc(OTf)_3]) \quad (1)$$

Cyclic voltammetry measurements were carried out to examine the effect of Sc^{3+} on the redox behavior of PTIO$^{\bullet}$ in deaerated MeCN containing 0.10 M Bu_4NClO_4. Two well-defined reversible redox waves were observed at −0.98 and +0.70 V vs. the saturated calomel electrode (SCE) for the one-electron reduction and oxidation of PTIO$^{\bullet}$ to produce $PTIO^-$ and $PTIO^+$, respectively, in the absence of Sc^{3+} (Figure 3). Thus, the separation between the one-electron oxidation and reduction potentials obtained in this study (1.68 V) is slightly smaller than the literature value (1.73 V) [35]. Upon the addition of 10 equiv. of $Sc(OTf)_3$, however, a drastic change was observed in the cyclic voltammogram (Figure 3). The reversible wave for the one-electron reduction of PTIO$^{\bullet}$ and the oxidation wave of PTIO$^{\bullet}$ disappeared, while a new oxidation peak appeared at +1.66 V vs. SCE. This new peak was assigned to the oxidation of $[(PTIO)Sc]^{2+}$, which was generated by the disproportionation of PTIO$^{\bullet}$ upon the addition of Sc^{3+}, to produce PTIO$^{\bullet}$ and Sc^{3+} (Scheme 4). Then, PTIO$^{\bullet}$ was further oxidized to $PTIO^+$ (Scheme 4). Although the reduction peak of PTIO$^{\bullet}$ in the presence of $Sc(OTf)_3$ could not be observed due to the disproportionation reaction, such a large (ca. 2.6 V) positive shift of the one-electron reduction potential of PTIO$^{\bullet}$ (equivalent to the oxidation peak for $PTIO^-$) upon the addition of $Sc(OTf)_3$ enables the disproportionation to occur.

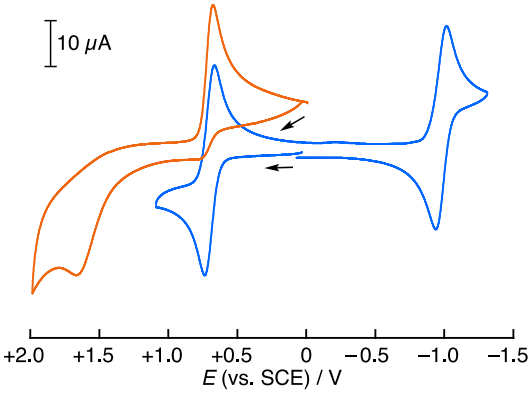

Figure 3. Cyclic voltammograms of PTIO$^{\bullet}$ (1.0×10^{-3} M) before (blue line) and after (orange line) the addition of $Sc(OTf)_3$ (1.0×10^{-2} M) in deaerated MeCN containing 0.10 M Bu_4NClO_4 recorded at the scan rate of 100 mV s^{-1} on a glassy carbon working electrode at 298 K. Arrows denote starting points and the direction of scanning.

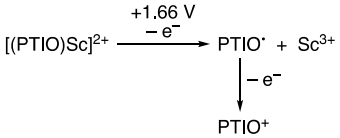

Scheme 4. Electrochemical oxidation of $[(PTIO)Sc]^{2+}$ at +1.66 V vs. SCE.

The reversibility of the disproportionation of PTIO$^{\bullet}$ by the addition of $Sc(OTf)_3$ has also been examined as in the case of DPPH$^{\bullet}$ [24]. The addition of H_2O to the PTIO$^{\bullet}$–$Sc(OTf)_3$ system in deaerated MeCN resulted in the increase in the absorption band at 361 nm due to PTIO$^{\bullet}$ (Figure 4) (Video S2 of the Supplementary Materials). This indicates that an electron-transfer comproportionation occurred to regenerate PTIO$^{\bullet}$. When H_2O was replaced by EtOH or MeOH, the regeneration of PTIO$^{\bullet}$ was also observed. However, the amount of the recovery was significantly lower compared to the case of H_2O.

The spectral change after the addition of H_2O (1.9 M) to a deaerated MeCN solution containing PTIO$^\bullet$ (6.9×10^{-5} M) and $Sc(OTf)_3$ (3.5×10^{-5} M) monitored by a stopped-flow technique is shown in Figure 5a. The time course change in the absorbance at 361 nm obeyed second-order kinetics (inset of Figure 5a), from which the observed second-order rate constant for the comproportionation (k_{comp}, comp: comproportionation) was determined to be 1.4×10^4 M^{-1} s^{-1}. The comproportionation reactions between reduced and oxidized forms of nitroxyl radicals, hydroxyl amines, and oxoammonium cations, respectively, have been extensively studied [58–66]. Goldstein et al. determined the k_{comp} value between the hydroxylamine and oxoammonium cation derived from TEMPO to be 5.2×10 M^{-1} s^{-1} in a phosphate-buffered solution, while the deprotonation of the hydroxylamine resulted in a significant increase in the k_{comp} value (3.3×10^4 M^{-1} s^{-1}) [59]. This suggests that the electron donor to $PTIO^+$ in this study is $PTIO^-$, rather than its protonated form (PTIOH). The k_{comp} value linearly increased with the increasing concentration of H_2O, as shown in Figure 5b. Thus, the H_2O-induced comproportionation reaction is shown in Scheme 5. It is suggested that the complex formation of Sc^{3+} with H_2O may weaken the interaction between $PTIO^-$ and Sc^{3+}, leading to the electron-transfer comproportionation regenerating PTIO$^\bullet$.

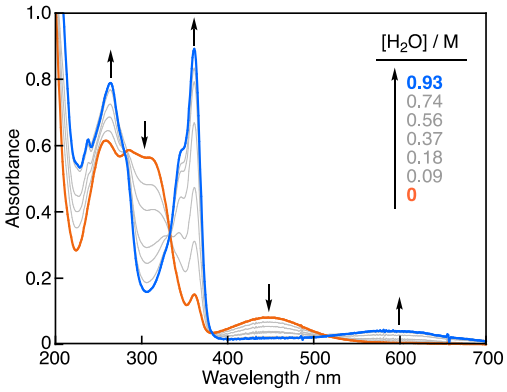

Figure 4. Spectral change upon the addition of H_2O to a deaerated MeCN solution of PTIO$^\bullet$ (7.3×10^{-5} M) and $Sc(OTf)_3$ (3.7×10^{-5} M) at 298 K. Orange and blue lines are the initial and final spectra, respectively. Arrows denote the direction of absorption changes.

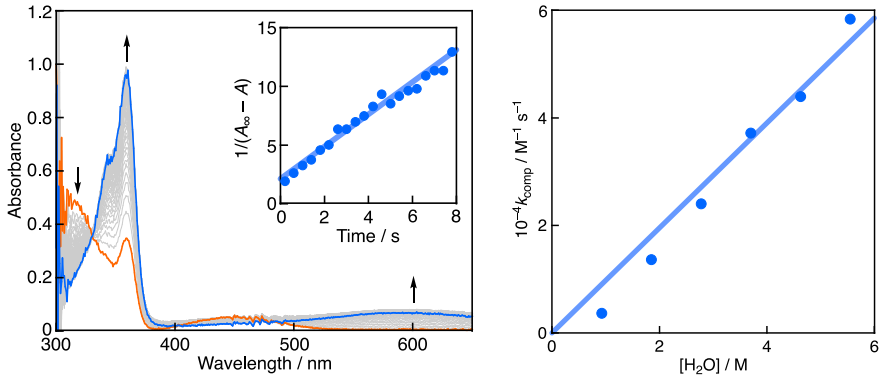

(**a**) (**b**)

Figure 5. (**a**) Spectral change (interval: 0.1 s) observed after the addition of H_2O (1.9 M) to a deaerated MeCN solution of PTIO$^\bullet$ (6.9×10^{-5} M) and $Sc(OTf)_3$ (3.5×10^{-5} M) at 298 K. Orange and blue lines are the initial and final spectra, respectively. Arrows denote the direction of absorption changes. Inset: the second-order plot of the absorbance at 361 nm. (**b**) Plot of k_{comp} vs. [H_2O].

$$PTIO^+ + [(PTIO)Sc]^{2+} + H_2O \longrightarrow 2PTIO^{\cdot} + [Sc(H_2O)]^{3+}$$

Scheme 5. H_2O-induced regeneration of PTIO$^\bullet$.

The reversible disproportionation of PTIO• was also confirmed by the electron paramagnetic resonance (EPR) spectroscopy. The well-resolved five lines with a g value of 2.0067 and a hyperfine coupling constant (a_N) of 0.75 mT were observed in the EPR spectrum of PTIO• in deaerated MeCN (Figure 6a). After 0.5 equiv. of $Sc(OTf)_3$ was added to the MeCN solution of PTIO•, the signal intensity was significantly decreased, as shown in Figure 6b, although a trace amount of PTIO• was observed. The addition of H_2O to this PTIO•–$Sc(OTf)_3$ system in deaerated MeCN resulted in the regeneration of PTIO•, which was confirmed by the increase in the EPR signal intensity due to PTIO• (Figure 6c).

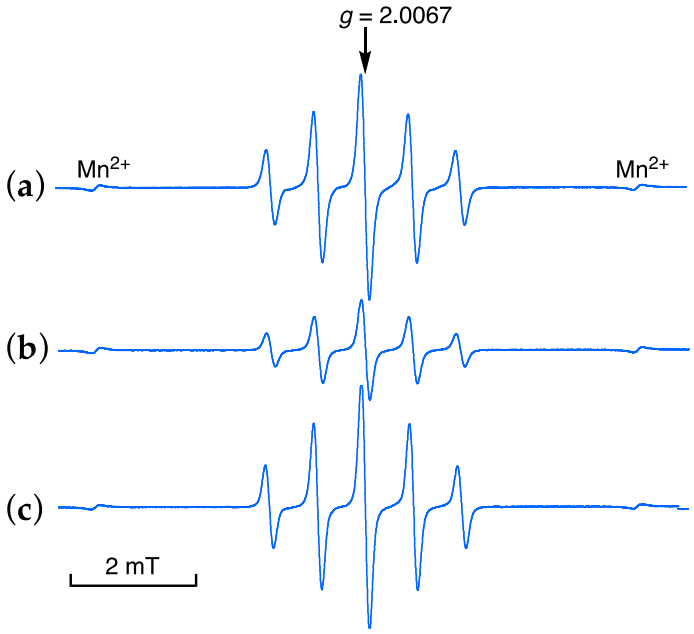

Figure 6. EPR spectra of (**a**) PTIO• (7.0×10^{-5} M), (**b**) PTIO• (7.0×10^{-5} M) after the addition of $Sc(OTf)_3$ (3.5×10^{-5} M), and (**c**) PTIO• (7.0×10^{-5} M) after the addition of $Sc(OTf)_3$ (3.5×10^{-5} M) and H_2O (5.6 M) in deaerated MeCN at room temperature.

3. Materials and Methods

3.1. Materials

PTIO• was commercially obtained from Tokyo Chemical Industry Co., Ltd., Tokyo, Japan. $Sc(OTf)_3$ was purchased from Sigma-Aldrich, St. Louis, MO, USA. MeCN, MeOH, and EtOH (spectral grade) used as solvents were commercially obtained from Nacalai Tesque, Inc., Kyoto, Japan, and used as received. Tetra-*n*-butylammonium perchlorate (Bu_4NClO_4), used as a supporting electrolyte for electrochemical measurements, was purchased from Tokyo Chemical Industry Co., Ltd., Tokyo, Japan, recrystallized from EtOH (spectral grade, Nacalai Tesque, Inc., Kyoto, Japan), and dried under vacuum at 313 K. The water used in this study was freshly prepared with a Milli-Q system (Millipore Direct-Q UV3) (Merch Millipore, Burlington, MA, USA).

3.2. Spectral and Kinetic Measurements

To avoid the effect of molecular oxygen (O_2), the reactions were carried out under strictly deaerated conditions, where a continuous flow of argon (Ar) gas was bubbled through each MeCN solution. Typically, a 10 µL of aliquot of $Sc(OTf)_3$ (1.3×10^{-3} M) in deaerated MeCN was added to a quartz cuvette (10 mm i.d.), which contained PTIO• (7.2×10^{-3} M) in deaerated MeCN. UV-vis spectral changes associated with the reaction were monitored using an Agilent 8453 photodiode array spectrophotometer thermostated with a Peltier temperature control at 298 K (Agilent Technologies, Santa Clara, CA, USA). The reaction rates were followed by monitoring the absorbance at 361 nm due to PTIO• after mixing of PTIO• in deaerated MeCN with a deaerated MeCN solution containing $Sc(OTf)_3$ at a volumetric ratio of 1:1 using a stopped-flow technique on a UNISOKU

RSP-1000-02NM stopped-flow spectrophotometer (UNISOK Co., Ltd., Osaka, Japan), which was thermostated with a Thermo Scientific NESLAB RTE-7 Circulating Bath (Thermo Fisher Scientific, Inc., Waltham, MA, USA) at 298 K. For the regeneration reaction of $PTIO^{\bullet}$, a deaerated MeCN solution containing H_2O were mixed with a deaerated MeCN solution of $PTIO^{\bullet}$ (1.4×10^{-4} M) and $Sc(OTf)_3$ (7.0×10^{-5} M) at a volumetric ratio of 1:1 using a stopped-flow technique. The observed second-order rate constants (k_{disp} and k_{comp}) were obtained by a least-square curve fit using an Apple MacBook Pro personal computer (Apple Inc., Cupertino, CA, USA) or an HP EliteDesk 800 G4 SFF (HP Inc., Palo Alto, CA, USA). The plots of $1/(A - A_\infty)$ vs. time (A and A_∞ are the absorbance at the reaction time and the final absorbance, respectively) were linear until three or more half-lives, with a correlation coefficient $\rho > 0.999$. The k_{disp} and k_{comp} values were calculated by Slope$(A_0 - A_\infty)/[PTIO^{\bullet}]_0$, where Slope is the slope of the linear plot of $1/(A - A_\infty)$ vs. time, and A_0 and $[PTIO^{\bullet}]_0$ are the initial absorbance at 361 nm and initial concentration of $PTIO^{\bullet}$, respectively. In each case, it was confirmed that the k_{disp} and k_{comp} values derived from at least three independent measurements agreed within experimental error of ±5%.

3.3. Electrochemical Measurements

The cyclic voltammetry measurements were performed on an ALS-630A electrochemical analyzer (BAS Co., Ltd., Tokyo, Japan) in deaerated MeCN containing 0.10 M Bu_4NClO_4 as a supporting electrolyte. The continuous flow of Ar gas was bubbled through each MeCN solution to avoid the effect of O_2. The glassy carbon working electrode (3 mm diameter) (BAS Co., Ltd., Tokyo, Japan) was polished with polishing alumina suspension (BAS Co., Ltd., Tokyo, Japan) and an alumina polishing pad (BAS Co., Ltd., Tokyo, Japan) and rinsed with methanol (FUJIFILM Wako Pure Chemical Corporation, Osaka, Japan) prior to each measurement. The counter electrode was a platinum wire (BAS Co., Ltd., Tokyo, Japan). The concentration of $PTIO^{\bullet}$ and $Sc(OTf)_3$ were 1.0×10^{-3} and 1.0×10^{-2} M, respectively. The measured potentials were recorded with respect to an $Ag/AgNO_3$ (0.01 M) reference electrode (BAS Co., Ltd., Tokyo, Japan) with a sweep rate of 100 mV s^{-1} at 298 K. The potentials were converted to those vs. the saturated calomel electrode (SCE) by adding 0.29 V [67].

3.4. EPR Measurements

The EPR spectra of $PTIO^{\bullet}$ (7.0×10^{-5} M) in the presence or absence of $Sc(OTf)_3$ (3.5×10^{-5} M) and/or H_2O (5.6 M) in deaerated MeCN were taken using a disposable RDC-60-S flat cell (inner size, 60 mm × 6 mm × 0.3 mm) (Flashpoint Ltd., Tokyo, Japan) on a JEOL X-band spectrometer (JES-RE1X) (JEOL Ltd., Tokyo, Japan) at room temperature under the following conditions: microwave frequency, 9.40 GHz; microwave power, 8 mW; center field, 333 mT; sweep width, 15 mT; sweep rate, 3 mT min^{-1}; modulation frequency, 100 kHz; modulation amplitude, 0.2 mT; and time constant, 0.1 s. EPR data acquisition was controlled by the WIN-RAD ESR Sata Analyzer System (Radical Research, Inc., Tokyo, Japan). The g values were calibrated with an Mn^{2+} marker. The experimental EPR spectra were analyzed and simulated using the WinSim 2002 software [68].

4. Conclusions

The Sc^{3+} with a strong Lewis acidity induced the electron-transfer disproportionation of $PTIO^{\bullet}$ in deaerated MeCN. The electrochemical measurements suggested that the significantly large positive shift of the one-electron reduction potential of $PTIO^{\bullet}$ in the presence of Sc^{3+} enables the disproportionation to occur. The addition of H_2O to the $PTIO^{\bullet}$–$Sc(OTf)_3$ system in deaerated MeCN resulted in the regeneration of $PTIO^{\bullet}$ because the complex formation of Sc^{3+} with H_2O weakened the interaction between $PTIO^{-}$ and Sc^{3+}. The drastic change in the redox reactivity of $PTIO^{\bullet}$ in the presence of Sc^{3+} as a strong Lewis acid provides not only valuable and fundamental information about the effects of the reaction environments on the reactivity of radical species but an excellent opportunity to develop radical-based redox flow batteries.

Supplementary Materials: The following supporting information can be downloaded at: https://www.mdpi.com/article/10.3390/ijms25084417/s1.

Author Contributions: Conceptualization, I.N.; methodology, S.F. and I.N.; formal analysis, Y.S. and H.I.; investigation, Y.S. and H.I.; validation, Y.S. and H.I.; resources, I.N.; data curation, Y.S., Y.T. and H.I.; writing—original draft preparation, I.N.; writing—review and editing, K.O., H.I., K.M. and S.F.; visualization, Y.S. and Y.T.; supervision, K.O., K.M., S.F. and I.N.; project administration, I.N.; funding acquisition, K.O., S.F. and I.N. All authors have read and agreed to the published version of the manuscript.

Funding: This work was partially supported by Grant-in-Aid (No. JP18K06620 to I.N., JP20H02779, JP20H04819, JP18H04650, JP17H03010, and JP16H02268 to K.O., and JP23K04686 to S.F.) from the Ministry of Education, Culture, Sports, Science and Technology, Japan.

Institutional Review Board Statement: Not applicable.

Informed Consent Statement: Not applicable.

Data Availability Statement: Data are contained within the article.

Conflicts of Interest: The authors declare no conflicts of interest.

Abbreviations

$Al(OTf)_3$	Aluminum triflate (OTf = OSO_2CF_3)
Bu_4NClO_4	Tetra-*n*-butylammonium perchlorate
$DPPH^{\bullet}$	2,2-Diphenyl-1-picrylhydrazyl
$DPPH^{-}$	One-electron-reduced species of $DPPH^{\bullet}$
$DPPH^{+}$	One-electron-oxidized species of $DPPH^{\bullet}$
EPR	Electron paramagnetic resonance
EtOH	Ethanol
MeCN	Acetonitrile
MeOH	Methanol
$^{\bullet}NO$	Nitric oxide
$PTIO^{\bullet}$	2-Phenyl-4,4,5,5-tetramethylimidazoline-1-oxyl 3-oxide
$PTIO^{-}$	One-electron-reduced species of $PTIO^{\bullet}$
$PTIO^{+}$	One-electron-oxidized species of $PTIO^{\bullet}$
PTIOH	Protonated form of $PTIO^{-}$
SCE	Saturated calomel electrode
$Sc(OTf)_3$	Scandium triflate (OTf = OSO_2CF_3)
TEMPO	2,2,6,6-Tetramethylpiperidyl-1-oxyl

References

1. Fukuzumi, S.; Ohkubo, K. Metal ion-coupled and decoupled electron transfer. *Coord. Chem. Rev.* **2010**, *254*, 372–385. [CrossRef]
2. Ghosh, T.K.; Maity, S.; Ghosh, S.; Gomila, R.M.; Frontera, A.; Ghosh, A. Role of redox-inactive metal ions in modulating the reduction potential of uranyl Schiff base complexes: Detailed experimental and theoretical studies. *Inorg. Chem.* **2022**, *61*, 7130–7142. [CrossRef]
3. Mukai, K.; Nakamura, A.; Nagaoka, S.; Ouchi, A.; Azuma, N. Notable effects of the metal salts on the quenching reaction of singlet oxygen by α-tocopherol in ethanol solution. *Bull. Chem. Soc. Jpn.* **2015**, *88*, 1503–1510. [CrossRef]
4. Mukai, K.; Kohno, Y.; Ouchi, A.; Nagaoka, S. Notable effect of metal salts on UV-vis absorption spectra of α-, β-, γ-, and δ-tocopheroxyl radicals in acetonitrile solution. The complex formation between tocopheroxyls and metal cations. *J. Phys. Chem. B* **2012**, *116*, 8930–8941. [CrossRef]
5. Mukai, K.; Oi, M.; Ouchi, A.; Nagaoka, S. Kinetic study of the α-tocopherol-regeneration reaction of ubiquinol-10 in methanol and acetonitrile solutions: Notable effect of the alkali and alkaline earth metal salts on the reaction rates. *J. Phys. Chem. B* **2012**, *116*, 2615–2621. [CrossRef]
6. Kohno, Y.; Fujii, M.; Matsuoka, C.; Hashimoto, H.; Ouchi, A.; Nagaoka, S.; Mukai, K. Notable effects of the metal salts on the formation and decay reactions of α-tocopheroxyl radical in acetonitrile solution. The complex formation between α-tocopheroxyl radical and metal cations. *J. Phys. Chem. B* **2011**, *115*, 9880–9888. [CrossRef]
7. Ouchi, A.; Nagaoka, S.; Abe, K.; Mukai, K. Kinetic study of the aroxyl radical-scavenging reaction of α-tocopherol in methanol solution: Notable effect of the alkali and alkaline earth metal salts on the reaction rates. *J. Phys. Chem. B* **2009**, *113*, 13322–13331. [CrossRef]

8. Ngueumaleu, Y.; Deutchoua, A.D.D.; Hanga, S.S.P.; Liendji, R.W.; Dedzo, G.K.; Ngameni, E. Probing the reactivity of 2,2-diphenyl-1-picrylhydrazyl (DPPH) with metal cations and acids in acetonitrile by electrochemistry and UV-vis spectroscopy. *Phys. Chem. Chem. Phys.* **2023**, *25*, 5282–5290. [CrossRef]
9. Deutchoua, A.D.D.; Ngueumaleu, Y.; Liendji, R.W.; Sonita, S.; Hanga, P.; Nguelo, B.B.; Dedzo, G.K.; Ngameni, E. Unusual reactivity of 2,2-diphenyl-1-picrylhydrazyl (DPPH) with Fe^{3+} controlled by competing reactions. *RSC Adv.* **2024**, *14*, 1354–1359. [CrossRef]
10. Yuasa, J.; Fukuzumi, S. Off-off-on switching of fluorescence and electron transfer depending on stepwise complex formation of a host ligand with guest metal ions. *J. Am. Chem. Soc.* **2008**, *130*, 566–575. [CrossRef]
11. Fukuzumi, S.; Yuasa, J.; Satoh, N.; Suenobu, T. Scandium ion-promoted photoinduced electron transfer from electron donors to acridine and pyrene. Essential role of scandium ion in photocatalytic oxygenation of hexamethylbenzene. *J. Am. Chem. Soc.* **2004**, *126*, 7585–7594. [CrossRef]
12. Fukuzumi, S.; Fujii, Y.; Suenobu, T. Metal ion-catalyzed cycloaddition vs. hydride transfer reactions of NADH analogues with *p*-benzoquinone. *J. Am. Chem. Soc.* **2001**, *123*, 10191–10199. [CrossRef]
13. Zeng, Y.; Zhang, G.; Zhang, D.; Zhu, D. A new tetrathiafulvalene–quinone–tetrathiafulvalene triad: Modulation of the intramolecular charge transfer by the electron-transfer process promoted by metal ions. *J. Org. Chem.* **2009**, *74*, 4375–4378. [CrossRef]
14. Zhao, B.-T.; Peng, Q.-M.; Zhu, X.-M.; Yan, Z.-N.; Zhu, W.-M. Metal-promoted intermolecular electron transfer in tetrathiafulvalene–thiacalix[4]arene conjugates and tetrachlorobenzoquinone. *J. Org. Chem.* **2015**, *80*, 1052–1058. [CrossRef]
15. Mühldorf, B.; Wolf, R. Photocatalytic benzylic C–H bond oxidation with a flavin scandium complex. *Chem. Commun.* **2015**, *51*, 8425–8428. [CrossRef]
16. Sankaralingam, M.; Lee, Y.-M.; Pineda-Galvan, Y.; Karmalkar, D.G.; Seo, M.S.; Jeon, S.H.; Pushkar, Y.; Fukuzumi, S.; Nam, W. Redox reactivity of a mononuclear manganese-oxo complex binding calcium ion and other redox-inactive metal ions. *J. Am. Chem. Soc.* **2019**, *141*, 1324–1336. [CrossRef]
17. Kojima, T.; Kobayashi, R.; Ishizuka, T.; Yamakawa, S.; Kotani, H.; Nakanishi, T.; Ohkubo, K.; Fukuzumi, S. Binding of scandium ions to metalloporphyrin–Flavin complexes for long-lived charge separation. *Chem. Eur. J.* **2014**, *20*, 15518–15532. [CrossRef]
18. Kaur, S.; Bera, M.; Santra, A.; Munshi, S.; Sterbinsky, G.E.; Wu, T.; Moonshiram, D.; Paria, S. Effect of redox-inactive metal ion–nickel(III) interactions on the redox properties and proton-coupled electron transfer reactivity. *Inorg. Chem.* **2022**, *61*, 14252–14266. [CrossRef]
19. Devi, T.; Lee, Y.-M.; Nam, W.; Fukuzumi, S. Metal ion-coupled electron-transfer reactions of metal-oxygen complexes. *Coord. Chem. Rev.* **2020**, *410*, 213219. [CrossRef]
20. Liu, U.; Lau, T.-C. Activation of metal oxo and nitrido complexes by Lewis acids. *J. Am. Chem. Soc.* **2019**, *141*, 3755–3766. [CrossRef]
21. Pfaff, F.F.; Kundu, S.; Risch, M.; Pandian, S.; Heims, F.; Pryjomska-Ray, I.; Haack, P.; Metzinger, R.; Bill, E.; Dau, H.; et al. An oxocobalt(IV) complex stabilized by Lewis acid interactions with scandium(III) ions. *Angew. Chem. Int. Ed.* **2011**, *50*, 1711–1715. [CrossRef]
22. Fukuzumi, S.; Ohkubo, K. Quantitative evaluation of Lewis acidity of metal ions derived from the *g* values of ESR spectra of superoxide: Metal ion complexes in relation to the promoting effects in electron transfer reactions. *Chem. Eur. J.* **2000**, *6*, 4532–4535. [CrossRef]
23. Nakanishi, I.; Kawashima, T.; Ohkubo, K.; Waki, T.; Uto, Y.; Kamada, T.; Ozawa, T.; Matsumoto, K.; Fukuzumi, S. Disproportionation of a 2,2-diphenyl-1-picrylhydrazyl radical as a model of reactive oxygen species catalysed by Lewis and/or Brønsted acids. *Chem. Commun.* **2014**, *50*, 814–816. [CrossRef]
24. Nakanishi, I.; Shoji, Y.; Ohkubo, K.; Ito, H.; Fukuzumi, S. Water-induced regeneration of a 2,2-diphenyl-1-picrylhydrazyl radical after its scandium ion-promoted electron-transfer disproportionation in an aprotic medium. *Molecules* **2023**, *28*, 5002. [CrossRef]
25. Jiang, S.; Xie, Y.; Xie, Y.; Yu, L.-J.; Yan, X.; Zhao, F.-G.; Mudugamuwa, C.J.; Coote, M.L.; Jia, X.; Zhang, K. Lewis acid-induced reversible disproportionation o TEMPO enables aqueous aluminum radical batteries. *J. Am. Chem. Soc.* **2023**, *145*, 14519–14528. [CrossRef]
26. Akaike, T.; Maeda, H. Quantitation of nitric oxide using 2-phenyl-4,4,5,5-tetramethylimizazoline-1-oxyl 3-oxide (PTIO). *Methods Enzymol.* **1996**, *268*, 211–221.
27. Akaike, T.; Yoshida, M.; Miyamoto, Y.; Sato, K.; Kohno, M.; Sasamoto, K.; Miyazaki, K.; Ueda, S.; Maeda, H. Antagonistic action of imidazolineoxyl *N*-oxide against endothelium-derived relaxing factor/$^{\bullet}$NO through a radical reaction. *Biochemistry* **1993**, *32*, 827–832. [CrossRef]
28. Sueishi, Y.; Hori, M.; Kita, M.; Kotake, Y. Nitric oxide (NO) scavenging capacity of natural antioxidants. *Food Chem.* **2011**, *129*, 866–870. [CrossRef]
29. Fricker, S.P. Nitric oxide scavengers as a therapeutic approach to nitric oxide mediated disease. *Expert Opin. Invesitig. Drugs* **1999**, *8*, 1209–1222. [CrossRef]
30. Kovaleva, V.D.; Uzdensky, A.B. Photodynamic therapy-induced nitric oxide production in neuronal and glial cells. *J. Biomed. Opt.* **2016**, *21*, 105005. [CrossRef]

31. Perlikowski, D.; Lechowicz, K.; Pawłowicz, I.; Arasimonwicz-Jelonek, M.; Kosmala, A. Scavenging of nitric oxide up-regulates photosynthesis under drought in *Festuca arundinacea* and *F. glaucescens* but reduces their drought tolerance. *Sci. Rep.* **2022**, *12*, 6500. [CrossRef]
32. Fu, J.; Chu, X.; Sun, Y.; Miao, Y.; Xu, Y.; Hu, T. Nitric oxide mediates 5-aminolevulinic acid-induced antioxidant defense in leaves of *Elymus nutans* griseb. exposed to chilling stress. *PLoS ONE* **2015**, *10*, e0130367. [CrossRef]
33. Goldstein, S.; Russo, A.; Samuni, A. Reactions of PTIO and carboxy-PTIO with $^{\bullet}NO$, $^{\bullet}NO_2$, and $O_2^{\bullet-}$. *J. Biol. Chem.* **2003**, *278*, 50949–50955. [CrossRef]
34. Joseph, J.; Kalyanaraman, B.; Hyde, J.S. Trapping of nitric oxide by nitronyl nitroxides: An electron spin resonance investigation. *Biochem. Biophys. Res. Commun.* **1994**, *192*, 926–934. [CrossRef]
35. Duan, W.; Vemuri, R.S.; Milshtein, J.D.; Laramie, S.; Dmello, R.D.; Huang, J.; Zhang, L.; Hu, D.; Vijayakumar, M.; Wang, W.; et al. A symmetric organic-based nonaqueous redox flow battery and its state of charge diagnostic by FTIR. *J. Mater. Chem. A* **2016**, *4*, 5448–5456. [CrossRef]
36. Tkacheva, A.; Sun, B.; Zhang, J.; Wang, G.; McDonagh, M. Nitronyl nitroxide-based redox mediators for Li-O_2 batteries. *J. Phys. Chem. C* **2021**, *125*, 2824–2830. [CrossRef]
37. Sinclair, N.S.; Poe, D.; Savinell, R.F.; Maginn, E.J.; Wainright, J.S. A nitroxide containing organic molecule in a deep eutectic solvent for flow battery applications. *J. Electrochem. Soc.* **2021**, *168*, 020527. [CrossRef]
38. Zou, X.; Wu, Q.; Li, Z.; Zhang, S.; Dong, L.; Chen, Y.; Dai, Y.; Ji, C.; Liang, H.; Lin, X. *Lactiplantibacillus plantarum* A72, a strain with antioxidant properties, obtained through ARTP mutagenesis, affects *Caenorhabditis elegans* anti-aging. *Foods* **2024**, *13*, 924. [CrossRef]
39. Li, X.; Han, W.; He, G.; Yang, J.; Li, J.; Ma, H.; Wang, S. Hydrogel-transformable antioxidant poly-γ-glutamic acid/polyethyleneimine hemostatic powder for efficient wound hemostasis. *Gels* **2024**, *10*, 68. [CrossRef]
40. Ke, Q.; Wang, H.; Xiao, Y.; Kou, X.; Chem, F.; Meng, Q.; Gao, W. A novel water-soluble polysaccharide from daylily (*Hemerocallis citrina* baroni): Isolation, structure analysis, and probiotics adhesion promotion effect. *Food* **2024**, *13*, 721. [CrossRef]
41. Li, X.; Ouyang, X.; Chen, B.; Liu, S.; Zeng, J. Linkage and stereochemistry characters of phenolic antioxidant product formation. *J. Agric. Food Chem.* **2023**, *71*, 5382–5390.
42. Lu, H.; Wei, J.; Liu, K.; Li, Z.; Xu, T.; Yang, D.; Gao, Q.; Xiang, H.; Li, G.; Chen, Y. Radical-scavenging and subchondral bone-regenerating nanomedicine for osteoarthritis treatment. *ACS Nano* **2023**, *17*, 6131–6146. [CrossRef]
43. Wang, J.; Xue, X.; Miao, X. Antioxidant effects of quercetin nanocrystals in nanosuspension against hydrogen peroxide-induced oxidative stress in a zebrafish model. *Pharmaceuticals* **2023**, *16*, 1209. [CrossRef]
44. Qi, Y.; Huang, Y.; Dong, Y.; Zhang, W.; Xia, F.; Bai, H.; Stevanovic, Z.D.; Li, H.; Shi, L. Effective improvement of the oxidative stability of *Acer truncatum* bunge seed oil, a new woody oil food resource, by rosemary extract. *Antioxidants* **2023**, *12*, 889. [CrossRef]
45. Gong, J.; Liu, Q.; Cai, L.; Yang, Q.; Tong, Y.; Chen, X.; Kotha, S.; Mao, X.; He, W. Multimechanism collaborative superior antioxidant CDzymes to alleviate salt stress-induced oxidative damage in plant growth. *ACS Sustain. Chem. Eng.* **2023**, *11*, 4237–4247.
46. Wang, Y.; Huo, L.; Jia, Q.Q.; Jin, L. Preparation and evaluation of antioxidant activity of citric acid-polyethylene glycol-tannin elastomers. *Colloid Polym. Sci.* **2023**, *301*, 1351–1363.
47. Chen, B.; Li, X.; Ouyang, X.; Liu, J.; Liu, Y.; Chen, D. Comparison of ferroptosis-inhibitory mechanisms between ferrostatin-1 and dietary stilbene (piceatannol and astringin). *Molecules* **2021**, *26*, 1092. [CrossRef]
48. Zhang, W.; Li, X.; Hua, Y.; Li, Z.; Chen, B.; Liu, A.; Lu, W.; Zhao, X.; Diao, Y.; Chen, D. Antioxidant product analysis of *Hulu Tea* (*Tadehagi triquetrum*). *New J. Chem.* **2021**, *45*, 20257–20265.
49. Li, X.; Zeng, J.; Liu, Y.; Liang, M.; Liu, Q.; Li, Z.; Zhao, X.; Chen, D. Inhibitory effect and mechanism of action of quercetin and quercetin Diels-Alder *anti*-dimer on erastin-induced ferroptosis in bone marrow-derived mesenchymal stem cells. *Antioxidants* **2020**, *9*, 205. [CrossRef] [PubMed]
50. He, H.; Shi, X.; Wang, J.; Wang, X.; Wang, Q.; Yu, D.; Ge, B.; Zhang, X.; Huang, F. Reactive oxygen species-induced aggregation of nanoqymes for neuron injury. *ACS Appl. Mater. Interfaces* **2020**, *12*, 209–216. [CrossRef] [PubMed]
51. Ouyang, X.; Li, X.; Liu, J.; Liu, Y.; Xie, Y.; Du, Z.; Xie, H.; Chen, X.; Lu, W.; Chen, D. Structure-activity relationship and mechanism of four monostilbenes with respect to ferroptosis inhibition. *RSC Adv.* **2020**, *10*, 31171–31179. [CrossRef]
52. Li, X.; Liu, J.; Chen, B.; Chen, Y.; Dai, W.; Li, Y.; Zhu, M. Covalent bridging of corilagin improves antiferroptosis activity: Comparison with 1,3,6-tri-*O*-galloyl-β-D-glucopyranose. *ACS Med. Chem. Lett.* **2020**, *11*, 2232–2237. [CrossRef]
53. Li, X.; Chen, B.; Zhao, X.; Chen, D. 2-Phenyl-4,4,5,5-tetramethylimidazoline-1-oxyl 3-oxide (PTIO•) trapping activity and mechanisms of 16 phenolic xanthones. *Molecules* **2018**, *23*, 1692. [CrossRef]
54. Li, X.; Chen, B.; Xie, H.; HE, Y.; Zhong, D.; Chen, D. Antioxidant structure-activity relationship analysis of five dihydrochalcones. *Molecules* **2018**, *23*, 1162. [CrossRef]
55. Li, X.; Li, K.; Xie, H.; Xie, Y.; Li, Y.; Zhao, X.; Jiang, X.; Chen, D. Antioxidant and cytoprotective effects of the di-*O*-caffeoylqunic acid family: The mechanism, structure–activity relationship, and conformational effect. *Molecules* **2018**, *23*, 222. [CrossRef]
56. Li, X. 2-Phenyl-4,4,5,5-tetramethylimidazoline-1-oxyl 3-oxide (PTIO$^{\bullet}$) radical scavenging: A new and simple antioxidant assay *in vitro*. *J. Agric. Food Chem.* **2017**, *65*, 6288–6297. [CrossRef]

57. Zhu, M.; Wang, S.; Li, Z.; Li, J.; Xu, Z.; Liu, X.; Huang, X. Tyrosine residues initiated photopolymerization in living organisms. *Nat. Commun.* **2023**, *14*, 3598. [CrossRef]
58. Samuni, U.; Samuni, Y.; Goldstein, S. On the distinction between nitroxyl and nitric oxide using nitronyl nitroxides. *J. Am. Chem. Soc.* **2010**, *132*, 8428–8432. [CrossRef]
59. Israeli, A.; Pratt, M.; Oron, M.; Samuni, A.; Kohen, R.; Goldstein, S. Kinetics and mechanism of the comproportionation reaction between oxoammonium cation and hydroxylamine derived from cyclic nitroxides. *Free Radic. Biol. Med.* **2005**, *38*, 317–324. [CrossRef]
60. Zhang, R.L.; Goldstein, S.; Samuni, A. Kinetics of superoxide-induced exchange among nitroxide antioxidants and their oxidized and reduced forms. *Free Radic. Biol. Med.* **1999**, *26*, 1245–1252. [CrossRef]
61. Zhang, R.; Pinson, A.; Samuni, A. Both hydroxylamine and nitroxide protect cardiomyocytes from oxidative stress. *Free Radic. Biol. Med.* **1998**, *24*, 66–75. [CrossRef]
62. Golubev, V.A.; Sen, V.D.; Kulyk, I.V.; Aleksandrov, A.L. Mechanism of the oxygen disproportionation of di-*tert*-alkylnitroxyl radicals. *Izv. Akad. Nauk SSSR Ser. Khim.* **1975**, *10*, 2235–2243.
63. Zauche, T.H.; Espenson, J.H. Kinetics of oxidation and comproportionation reactions involving an oxoammonium ion, benzyl alcohol and methyltirioxorhenium(VII). *Int. J. Chem. Kinet.* **1999**, *31*, 381–385. [CrossRef]
64. Dikalov, S.I.; Dikalova, A.E.; Mason, R.P. Noninvasive diagnostic tool for inflammation-induced oxidative stress using electron spin resonance spectroscopy and an extracellular cyclic hydroxylamine. *Arch. Biochem. Biophys.* **2002**, *402*, 218–226. [CrossRef]
65. Sen', V.D.; Tikhonov, I.V.; Borodin, L.I.; Pliss, E.M.; Golubev, V.A.; Syroeshkin, M.A.; Rusakov, A.I. Kinetics and thermodynamics of reversible disproportionation–comproportionation in redox triad oxoammonium cations-nitroxyl radicals-hydroxylamines. *J. Phys. Org. Chem.* **2015**, *28*, 17–24. [CrossRef]
66. Sen, V.D.; Golubev, V.A. Kinetics and mechanism for acid-catalyzed disproportionation of 2,2,6,6-tetramethylpiperidine-1-oxyl. *J. Phys. Org. Chem.* **2009**, *22*, 138–143. [CrossRef]
67. Mann, C.K.; Barnes, K.K. *Electrochemical Reactions in Nonaqueous Systems*; Marcel Dekker Inc.: New York, NY, USA, 1990.
68. Duling, D.R. Simulation of multiple isotropic spin-trap EPR spectra. *J. Magn. Reson. Ser. B* **1994**, *104*, 105–110. [CrossRef]

Disclaimer/Publisher's Note: The statements, opinions and data contained in all publications are solely those of the individual author(s) and contributor(s) and not of MDPI and/or the editor(s). MDPI and/or the editor(s) disclaim responsibility for any injury to people or property resulting from any ideas, methods, instructions or products referred to in the content.